Earth and Planetary Science Letters 290 (2010) 319–330

Contents lists available at ScienceDirect

Earth and Planetary Science Letters

journal homepage: www.elsevier.com/locate/epsl

Obscuring of long eccentricity cyclicity in Pleistocene oceanic carbon isotope records

Pinxian Wang [a,*], Jun Tian [a], Lucas J. Lourens [b]

[a] State Key Laboratory of Marine Geology, Tongji University, Shanghai, China
[b] Faculty of Geosciences, Department of Earth Sciences, Utrecht University, Utrecht, Netherlands

ARTICLE INFO

Article history:
Received 9 February 2009
Received in revised form 10 December 2009
Accepted 14 December 2009
Available online 13 January 2010

Editor: M.L. Delaney

Keywords:
long eccentricity
carbon isotope
oceanic carbon reservoir
Pliocene
Pleistocene
Ocean Drilling Program

ABSTRACT

Long eccentricity (400-kyr) cycles in carbon isotope records from the Pacific and Atlantic oceans and the Mediterranean sea of the past 5.0 Ma are compared. All records show maximum $\delta\delta^{13}$C values (δ^{13}Cmax) at eccentricity minima during the Pliocene, but this relationship obscured in the Pleistocene after ~1.6 Ma in particular for the open ocean deep-water δ^{13}C records. Since a clear anti-phase relationship was set up between oceanic δ^{18}O and δ^{13}C in the 100-kyr band from this time, we attribute the obscured 400-kyr signal to a major change in the oceanic carbon reservoir probably associated with restructure of the Southern Ocean. A similar change occurred in the Miocene at 13.9 Ma when the 400-kyr cyclicity in δ^{13}C records flattened out together with a drastic cooling and Antarctic ice-sheet expansion. A remarkable exception is the Mediterranean surface water δ^{13}C record, which remained paced by the long-term eccentricity cycle throughout the Pliocene and Pleistocene, suggesting a low-latitude climatic origin of the 400-kyr signal that is independent of glacial–interglacial forcing. Since the Earth is currently passing through an eccentricity minimum, it is crucial to understand the nature of the δ^{13}Cmax events.

1. Introduction

With the quantitative paleoclimate records extending back from Pleistocene to Paleogene, the signal of 400-kyr cycles of long eccentricity becomes increasingly prominent in carbon and oxygen isotope time series. In particular, the long eccentricity cycles in δ^{13}C and δ^{18}O was likened to be the Earth's "heartbeat" during the Oligocene (23 Ma–33.9 Ma) (Pälike et al., 2006). Clear 400-kyr periodicity in δ^{13}C and δ^{18}O records has also been found in the Oligocene/Miocene (20.5–25.4 Ma) sections from Ceara Rise (Paul et al., 2000; Zachos et al., 2001) and sub-Antarctic South Atlantic (16–24 Ma) (Billups et al., 2004), as well as in two Middle Miocene (13.9–17 Ma) northwest and southeast subtropical Pacific records (Holbourn et al., 2005, 2007). The 400-kyr cycle is considered as "the tuning fork of geological time" (Matthews and Froelich, 2002) and used in cyclostratigraphic studies down to the early Mesozoic (e.g., Kent and Olsen, 1999) in the capacity of the most stable orbital parameter in the geological history (Laskar, 1990).

In a sharp contrast, the conspicuous absence of the long eccentricity signal in the Pleistocene ice-age records has raised the so-called "400-kyr problem" (Imbrie and Imbrie, 1980). Instead, a 500-kyr periodicity was detected first in foraminiferal (Briskin and Berggren, 1975) and later on in tropical carbonate records (Droxler et al., 1990; Bassinot et al., 1994a). Recently, oceanic δ^{13}C records revealed with a similar periodicity over the last 1 Myr and have been labeled as "super-cycles" (Wang et al., 2003, 2004), "long-term fluctuations" (Hoogakker et al., 2006), or "long-term changes in the global carbon reservoir" (Mohtadi et al., 2006). This has enhanced the enigma why the 400-kyr signal is not a main component of Pleistocene δ^{13}C and δ^{18}O records.

The recent increase of continuous, high-resolution deep-sea records over the last 5.3 Ma (e.g., Tian et al., 2002; Lourens et al., 2004) enabled us to follow the evolution track of the long eccentricity components in the paleoceanographic records through the Pliocene and Pleistocene. Since the 400-kyr cycles are much more pronounced in δ^{13}C than in δ^{18}O (Pälike et al., 2006; Holbourn et al., 2007), the present paper focuses particularly on δ^{13}C records. On the basis of this data comparison, we will argue that a major reorganization of the global oceanic circulation at around 1.6 Ma obscured the long eccentricity signal in open ocean δ^{13}C records.

2. Data and methods

Only a limited number of Ocean Drilling Program (ODP) sites have produced high-resolution δ^{13}C and δ^{18}O records of the entire Pliocene and Pleistocene. Even less sites are useful for our comparative study, because the δ^{13}C data is not always available; this explains the absence of high-latitude sites. The six time series used here (Fig. 1; Table 1), however, are quite representative as it includes both benthic and planktonic records, and covers open and marginal basins from the Atlantic and Pacific. The Mediterranean δ^{13}C record is presented here for the first time and reflects the counterpart of the Mediterranean stacked oxygen isotopic chronology

* Corresponding author.
E-mail address: pxwang@tongji.edu.cn (P. Wang).

0012-821X/$ – see front matter © 2009 Elsevier B.V. All rights reserved.
doi:10.1016/j.epsl.2009.12.028

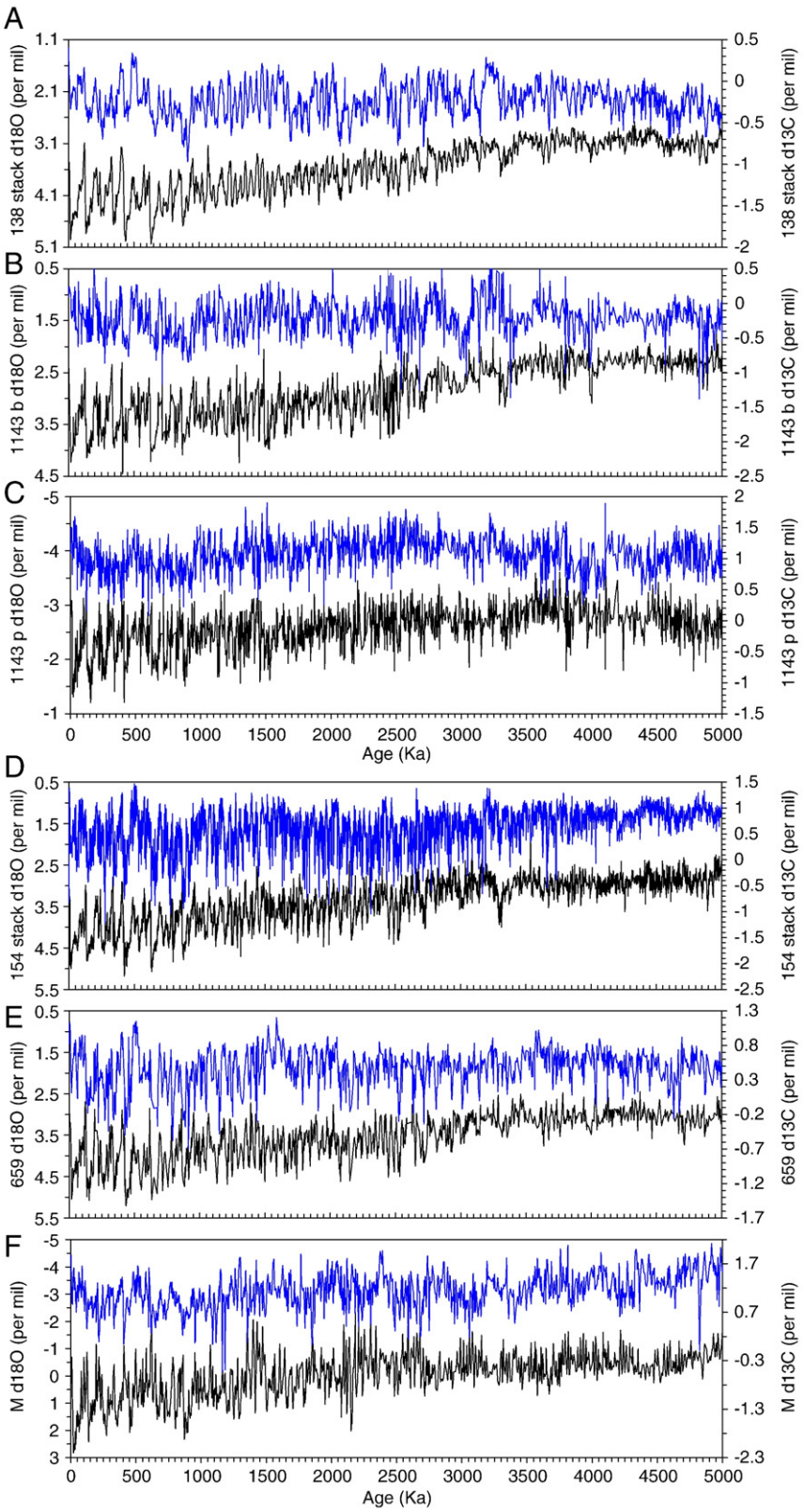

Fig. 1. Foraminiferal isotopic series for the past 5 Myr. Pacific region: (A), stacked benthic $\delta^{18}O$ and $\delta^{13}C$ of ODP Sites 846 and 849; (B), benthic $\delta^{18}O$ and $\delta^{13}C$ of ODP Site 1143; (C), planktonic $\delta^{18}O$ and $\delta^{13}C$ of ODP Site 1143; Atlantic region: (D), stacked benthic $\delta^{18}O$ and $\delta^{13}C$ of ODP Leg 154 (Site 926–929); (E), benthic $\delta^{18}O$ and $\delta^{13}C$ of ODP Site 659; Mediterranean sea: (F), stacked planktonic $\delta^{18}O$ and $\delta^{13}C$ (MD84641, KC01B, ODP Site 967 and the land-based marine successions of Vrica, Singa and Rossello). Note that blue lines denote $\delta^{13}C$ and black lines denote $\delta^{18}O$.

(Lourens et al., 2004). We included the Mediterranean records into our comparative study due to their sensitivity to orbital forcing (Lourens et al., 2004).

From the Pacific, we selected ODP Sites 846 and 849 on its eastern side (Shackleton et al., 1995; Mix et al., 1995a,b), and ODP 1143 from the South China Sea on its western side (Tian et al., 2002). ODP 1143 is

Table 1
Location of studied sites.

Ocean	Site	Location	Water depth (m)	Resolution (kyr)	References
West Pacific	1143	9°22′N 113°17′E	2772	2.6(P) 2.8(B)	This paper
	1146	19°27.40′N 116°16.37′E	2092	(4–5)	Holbourn et al. (2005)
East Pacific	846	3°06′S 90°49′W	3296	2.5	Shackleton et al. (1995)
	849	0°11′N 110°31′W	3851	4	Mix et al. (1995a,b)
	1218	8°53.378′N 135°22.00′W	4826	6	Wade and Pälike (2004)
Indian Ocean	721	16°40.6′N 59°51.9′E	1945	(1.2–3.5)	DeMenocal (1995)
	722	16°37.3′N 59°47.8′E	2028	(1.2–3.5)	
	758	5°23′N 90°21′E	2925	7	Chen et al. (1995); Farrell and Janecek (1991)
Atlantic Ocean	926	3°43.1′N 42°54.5′W	3598	3	Bickert et al. (1997); Tiedemann and Franz (1997); Franz and Tiedemann (1997); Shackleton and Hall (1997);
	927	5°27.7′N 44°28.8′W	3313	3	Billups et al. (1997); DeMenocal et al. (1997)
	928	5°27.3′N 43°44.9′W	4010	3	
	929	5°58.6′N 43°44.4′W	4357	3	
	607	41°00′N 32°58′W	3427	4	Raymo et al. (1989)
	659	18°05′N 21°02′W	3070	4	Tiedemann et al. (1994)
Mediterranean Sea	MD84641	33°02′N 32°38′E	1375	2	Fontugne and Calvert (1992)
	KC01B	36°15.25′N 17°44.34′E	3643	3	Rossignol-Strick and Paterne (1999)
	967	34°04′N 32°43.5′E	2553	3	Lourens et al. (1996a, 2004); Kroon et al. (1998)
	Vrica/Singa	Calabria, Italy	Land based	5	Lourens (2004)
	Rossello	Sicily, Italy	Land based	5	Kroon et al. (1998)

the only site where both benthic and planktonic isotopic records were generated for the last 5 Myr. We have averaged the $\delta^{18}O$ and $\delta^{13}C$ datasets of Sites 849 and 846. To correct for the mean difference between the $\delta^{13}C$ records, we added −0.219‰ to that of Site 849. The isotope chronology of Mix et al. (1995a) was followed for the last 1.812 Ma (Pleistocene). For the interval between 1.812 and 5.0 Ma, the initial SPB90-SCHPS95 timescale of (Shackleton et al., 1990, 1995) – which was based on tuning to the Ber90 astronomical solution (Laskar, 1988; Berger and Loutre, 1991) – was converted to the LR04 timescale (Lisiecki and Raymo, 2005) based on retuning (see also Lourens et al., 1996a) to the La04 solution (Laskar et al., 2004). Finally, a 3 kyr moving average was applied to smooth the $\delta^{18}O$ and $\delta^{13}C$ records.

Carbon and oxygen isotopic stacked records were constructed from the western equatorial Atlantic ODP Sites 926–929 (Franz and Tiedemann, 1997; Shackleton and Hall, 1997; Tiedemann and Franz, 1997, Bickert et al., 1997; Billups et al., 1997; DeMenocal et al., 1997). Both the eastern Pacific and the western equatorial Atlantic records were based on a variety of species, which were corrected for species offsets and equilibrated to seawater. The stacked records were linearly interpolated at 1 kyr steps and smoothed by a 3 kyr moving average.

From the eastern equatorial Atlantic we used ODP Site 659 (Tiedemann et al., 1994; Clemens and Tiedemann, 1997). The TSS94 timescale of ODP Site 659 was based 1) on tuning to the SPB90-SCHPS95 isotope chronology for the last 2.6 Myr and 2) on the correlation between maximum dust flux occurrences to minima in the Ber90 July summer insolation curve at 65°N between 2.6 and 5.2 Ma. We adopted the TSS94 timescale for the last 2.6 Myr, but retuned the dust flux maxima between 2.6 and 5.2 Ma to minima in the La04 65°N summer insolation curve.

The stacked Mediterranean dataset is represented by the stable isotopic records of the planktonic foraminiferal species *Globigerinoides ruber* from cores MD84641 (Fontugne and Calvert, 1992), KC01B (Rossignol-Strick and Paterne, 1999), ODP Site 967 (Lourens et al., 1996a, 2004; Kroon et al., 1998) and the land-based marine successions of Vrica, Singa and Rossello (Lourens et al., 1996b) (the stacked records are shown on the latest age model given by Lourens et al., 2004).

We applied cross-spectral analyses using the AnalySeries Program (Paillard et al., 1996) between the $\delta^{18}O$ and $\delta^{13}O$ records of each site and an astronomical target curve (ETP*) which was based on the sum of the normalized eccentricity, obliquity and climatic precession time series of the La04 solution in the ratio −1:−1:+0.5. Datasets were equally spaced and prepared by removing linear trends. Blackman–Tukey spectral analysis was carried out on 30% of the series between 0 and 5 Ma and 0 and 1.6 Ma using a Bartlett window and a Band Width of 0.001 and 0.0018, respectively. All spectra were normalized to unit variance. Gaussian filtering of each normalized and detrended series was carried out at frequency 0.002500 ± 0.000200.

3. Results

Cross-spectral analyses between the isotopic records and ETP* for the past 5.0 Myr revealed that most $\delta^{18}O$ spectra mark strong peaks in the obliquity (41-kyr) frequency band and to a lesser extent in that of precession (23.6-kyr, 22.4-kyr and 19-kyr) and short-term eccentricity (125-kyr, 95-kyr) (Fig. 2A and B). The obliquity-pacing of the deep ocean $\delta^{13}C$ and $\delta^{18}O$ records are generally attributed to glacial–interglacial variability throughout the Pliocene and Pleistocene (e.g. Imbrie et al., 1992; Shackleton et al., 1995). Phase estimates indicate

that maximum $\delta^{18}O_{ben}$ values and minimum $\delta^{13}C_{ben}$ values lag obliquity minima with 3–7 kyr (Table 2). A similar almost anti-phase relationship between $\delta^{18}O_{ben}$ and $\delta^{13}C_{ben}$ is found for the ~100-kyr glacial–interglacial rhythm of the late Pleistocene (Table 3).

With the exception of the Mediterranean no peak in the long-term eccentricity (400-kyr) band was found in any of the evaluated $\delta^{18}O$ records over the past 5.0 Ma (Fig. 2). This is in contrast to the $\delta^{13}C$ records, which clearly mark the imprint of the 400-kyr cycle in their individual spectra. In particular, high coherence (99% significance) occurs between ETP* and the $\delta^{13}C$ records of Leg 138, the Mediterranean and Site 659 with $\delta^{13}C$ values lagging long eccentricity minima by 6 to 40 kyr (Table 2). The coherences for the past 1.6 Ma are much lower for all sites, indicating that the 400-kyr component in the open ocean $\delta^{13}C$ became less prominent during this interval. Only the Mediterranean record yielded significant values for both $\delta^{13}C$ and $\delta^{18}O$ records (Table 3).

To further investigate the imprint of the 400-kyr cycle on the $\delta^{13}C$ record a comparison is made between the band-pass filters of the different sites and ETP* (Fig. 3A and B). Among the 6 sites studied, the late Pleistocene $\delta^{13}C$ curves of Site 1143 and Leg 154 are less amplified, and the $\delta^{13}C$ curves at site ODP 1143 are out of phase with eccentricity in the interval between 4 and 5 Ma. The Mediterranean $\delta^{13}C_{plan}$ reflects by far best the imprint of an almost in-phase long eccentricity cycle throughout the Pliocene and Pleistocene (Fig. 3B). Excluding the planktonic record of Site 1143, all $\delta^{13}C$ time series display clear 400-kyr cycles in the Pliocene part, which become less amplified, partly resulting from the edge effect of the band-pass filtering approach, and in a few cases somehow irregular during the middle to late Pleistocene (Fig. 3A and B). For instance, in the deep ocean records of Ceara Rise and the South China Sea two ~500-kyr cycles appear during the last million years. Consistent with the cross-spectral results (Table 2), Fig. 3 clearly shows that the filtered 400-kyr cycles of the $\delta^{13}C_{ben}$ records, with the exception of the stacked record of Leg 154, follow the long eccentricity component of the ETP* record with 30–50 kyr. A total of 13 long-term eccentricity-related $\delta^{13}C$ maximum events could be recognized in the Mediterranean $\delta^{13}C_{plan}$ record within the last 5 Ma, corresponding to long eccentricity minima and are numbered in a descending order (1–13 in Fig. 3). This picture is more complicated in the Pleistocene part in most of the other curves. A visual inspection shows, for example, that the $\delta^{13}C$max event at 0.5 Ma (Wang et al., 2004) surpasses that at 0.4 Ma, the last eccentricity minimum at all sites. In addition, $\delta^{13}C$max event No III (Wang et al., 2004) falls in between the eccentricity minima Nos. 3 and 4 and is associated with MIS 25–27. In result, only 12 $\delta^{13}C$max are observed at other sites (I–XII in Fig. 3; Table 4), with one $\delta^{13}C$max less in the Pleistocene. A tuning point in the long-term $\delta^{13}C$ cycles occurs at ~1.6 Ma, when the 400-kyr periodicity become blurry obscured. The last 1.6 Myr can be divided into three intervals that are separated by the $\delta^{13}C$max events at 1.0 Ma and 0.5 Ma (Wang et al., 2004; Hoogakker et al., 2006; Mohtadi et al., 2006) (Fig. 4B, D, F).

4. Discussion

4.1. Eccentricity pacing of $\delta^{13}C$ records

Eccentricity pacing of sedimentary sequences is known from deposits at least since the early Mesozoic (e.g., Olsen, 1986), but only limited isotope records are available beyond the Oligocene. High-resolution $\delta^{13}C$ records from the Paleocene–Eocene boundary sections in the Pacific, Atlantic and Southern Oceans yielded clear long-term eccentricity cycles in bulk-samples, and were used for orbital tuning (Cramer et al., 2003). A similar imprint of the 400-kyr and 100-kyr cycles on $\delta^{13}C$ and $\delta^{18}O$ records have been found in the Oligocene to Middle Miocene time interval (e.g. Wade and Pälike, 2004). A general feature in all these records is that $\delta^{13}C$ heavy values occur at long and short eccentricity minimum values, as illustrated by three time intervals in Fig. 5: the middle Oligocene from 26 to 30 Ma (Wade and Pälike, 2004), the Oligocene/Miocene transition from 21 to 24 Ma (Zachos et al., 2001) and the Middle Miocene from 13 to 17 Ma (Holbourn et al., 2004).

Zachos et al. (2001) argued that in an ice-free world eccentricity power appeared to be much more amplified in paleoclimate records, such as $\delta^{13}C$, than in the current Icehouse world. It has been proposed that in the ice-free early Paleogene, the ocean is much more homogeneous, and that the oceanic carbon reservoir responds directly to orbital forcing, mainly to the precession modulated by the eccentricity (Cramer et al., 2003; Lourens et al., 2005). In result, the hydrological and biogeochemical cycles respond to eccentricity in a correlated way. Because the residence time of carbon in the ocean–atmosphere–biosphere reservoir is $\sim 10^5$ yr, $\delta^{13}C$ changes in the global oceanic reservoir occur only on time scale $>10^5$ yr with a smoothing effect in lower frequencies (Cramer et al., 2003; Katz et al., 2005; Pälike et al., 2006). With the transfer from the Greenhouse to the Icehouse world, the insolation control of the global ice volume becomes the main driving force for $\delta^{18}O$ variations, but the basic pattern of the $\delta^{13}C$ variations on the long eccentricity time scale maintained at least until the Middle Miocene.

The significant 400-kyr pacing of Pliocene and Pleistocene deep ocean $\delta^{13}C$ records has previously been notified (e.g., Mix et al., 1995b). The observed time lag of 30–50 kyr with respect to long-term eccentricity is comparable to that observed for Miocene records (Holbourn et al., 2004). Among the Pliocene and Pleistocene $\delta^{13}C$ time series, highest coherence and an almost in-phase relationship between isotope records and long eccentricity cycles is found for the Mediterranean planktonic record (Fig. 3B). The 400-kyr $\delta^{13}C$max values in the Mediterranean record coincides with the periodically deposited thick homogeneous marl intervals between large sapropel groups during the Late Pliocene and Pleistocene or to the thick homogeneous $CaCO_3$-rich intervals in the Early Pliocene which were both linked to periods of minimum eccentricity values (Hilgen, 1991; Lourens et al., 1996a, 2004). Intervals of sapropel deposition have been associated with relatively humid circum-Mediterranean climate conditions and extensive Nile flooding related to an intensified African monsoon (e.g. Rossignol-Strick, 1983; Rohling and Hilgen, 1991). Depleted $\delta^{13}C$ values in planktonic foraminifers during sapropel formation have often been observed, and are generally linked to a combination of processes such as a shift in the isotopic composition of the dissolved inorganic carbon (DIC) due to mixing with the fresh water input (Gudjonsson and van der Zwaan, 1985; Fontugne and Calvert, 1992).

The strong influence of the 400-kyr cyclicity is not only restricted to the carbon isotope record of the Mediterranean, but seems evident in a number of low-latitude environmental records before 1.6 Ma such as aeolian detritus % in the Arabian Sea (Fig. 4H) (DeMenocal, 1995), dust flux in the Atlantic (Fig. 4I) (Tiedemann et al., 1994), and coccolithophore productivity (C_{37} alkenones concentration) in equatorial Pacific (Fig. 4J) (Lawrence et al., 2006). From the above listed proxies, the dust records are related to the African and Indian monsoons, and the productivity records to nutrient supply.

The strong imprint of the 400-kyr cyclicity in the low-latitude climate proxy records is interpreted in terms of a direct response to the low-latitude insolation changes and hence monsoon variability.

Fig. 2. Power spectra and cross-spectral results of the examined $\delta^{18}O$ and $\delta^{13}C$ records against ETP* for the past 5.0 Ma using the Analyseries software package (Paillard et al., 1996). (A) Data from Leg 138 and 154 and Site 659; (B) data from the Mediterranean and Site 1143. ETP* refers to the sum of the normalized eccentricity (multiplied by −1), obliquity (multiplied by −1) and climatic precession (multiplied by 0.5) time series derived from the La2004 solution (Laskar et al., 2004). All series were interpolated at 1-kyr and detrended. A parzen window was applied with 800 lags, which coincides with a bandwidth of 0.001875.

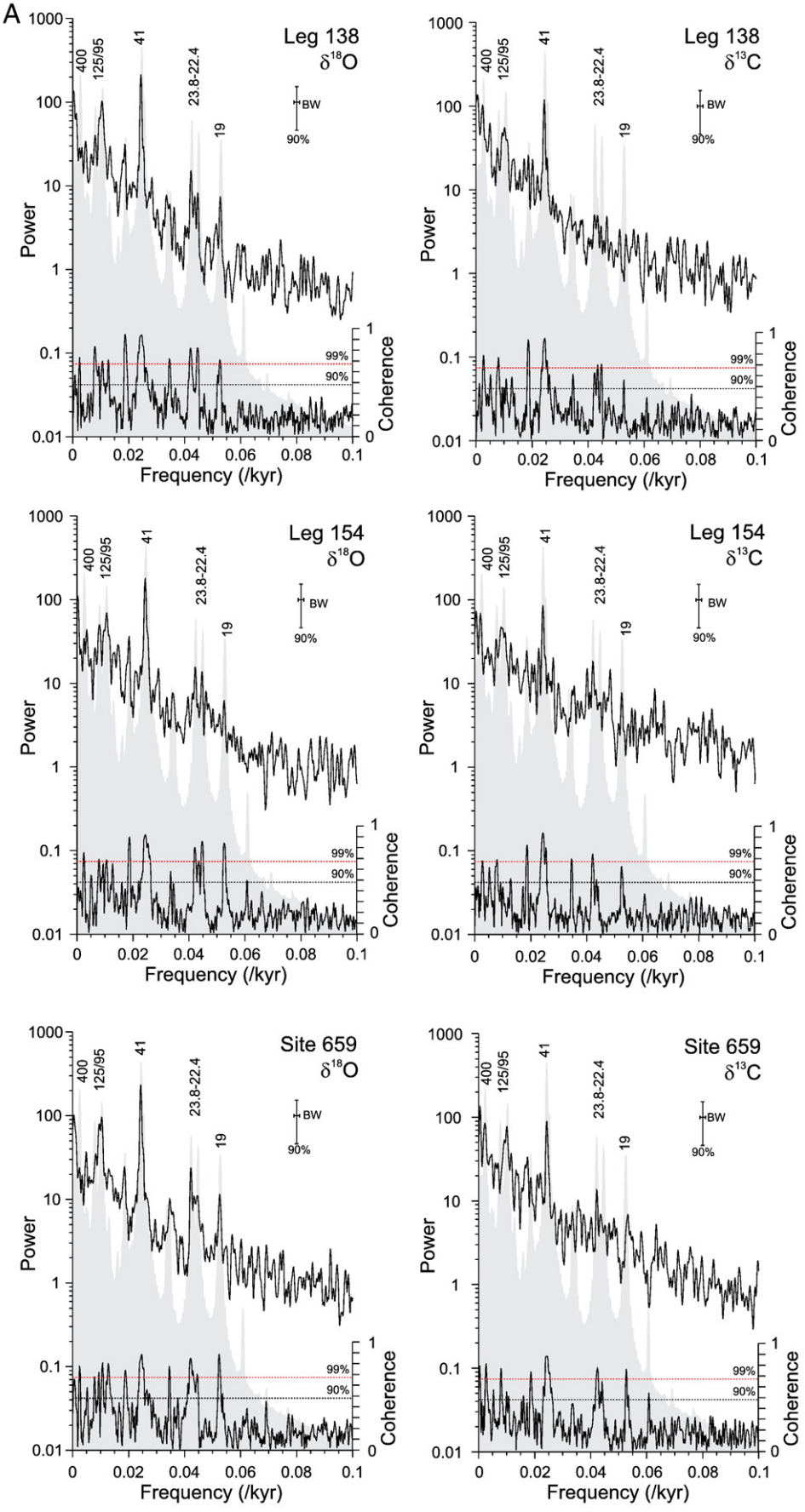
A
Leg 138
δ18O
Leg 138
δ13C
Leg 154
δ18O
Leg 154
δ13C
Site 659
δ18O
Site 659
δ13C
Power
Coherence
Frequency (/kyr)
400
125/95
41
23.8-22.4
19
BW
90%
99%

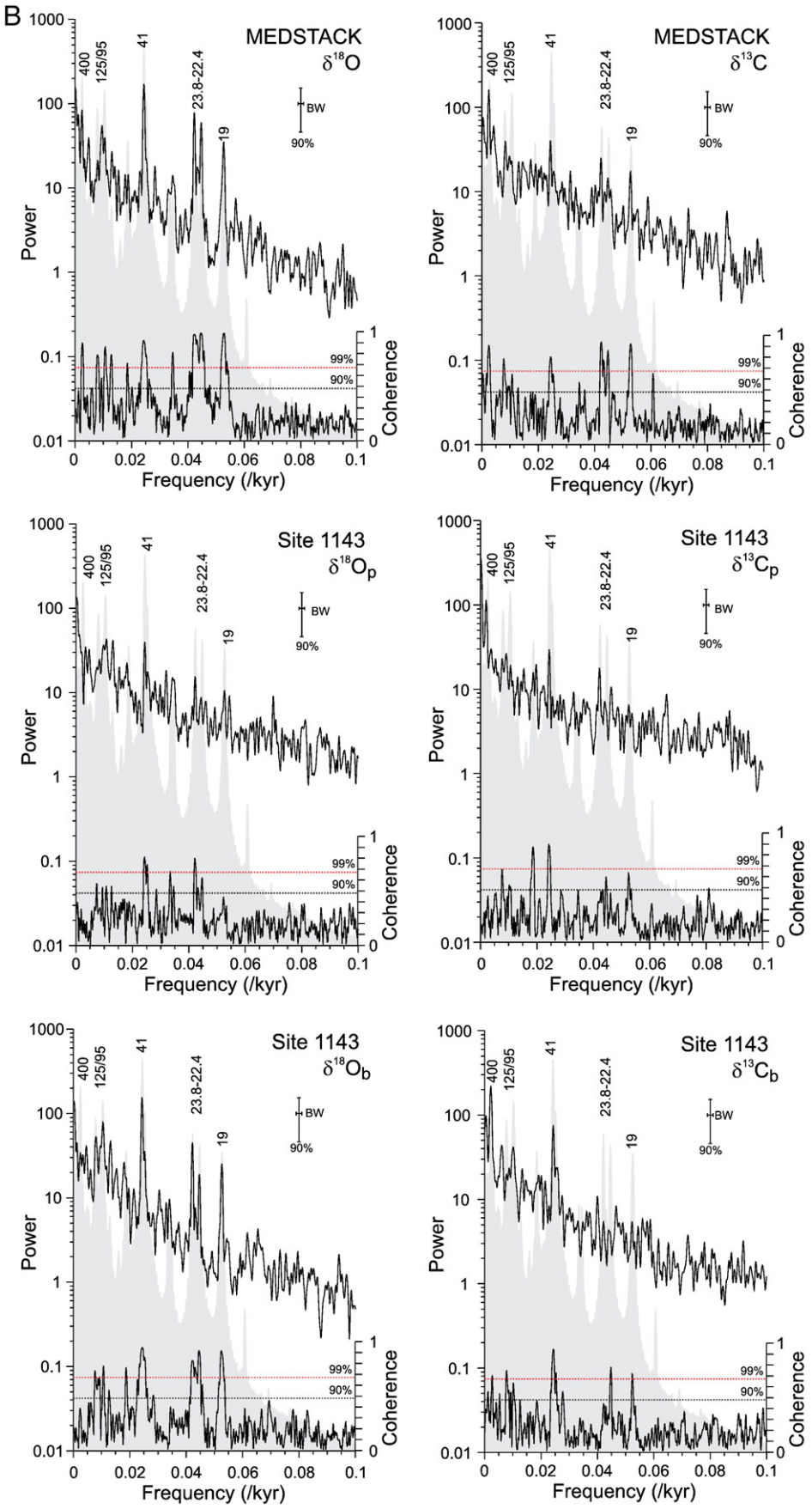

Fig. 2 (*continued*).

Table 2
Cross-spectral results between ETP* and stable isotope records (0–5.0 Ma).

	Eccentricity						Obliquity				Climatic precession			
	400 kyr		125 kyr		95 kyr		41 kyr		23.6 kyr		22.4 kyr		19 kyr	
	coh	pha	coh	pha	coh	pha	coh	pha	coh	pha	coh	pha	coh	pha
Leg 154														
$\delta^{18}O_{ben}$	**0.75**	−65±15	0.66	−10±19	**0.68**	19±17	**0.92**	21±7	**0.77**	15±14	**0.86**	−12±10	**0.84**	−36±11
$\delta^{13}C_{ben}$	0.57	−1±24	**0.69**	130±17	0.27	−173±61	**0.94**	−147±6	**0.71**	−133±16	0.20	76±89	0.59	−180±22
Leg 138														
$\delta^{18}O_{ben}$	**0.73**	−44±15	**0.83**	10±11	**0.69**	25±17	**0.94**	49±6	**0.79**	53±13	**0.81**	74±12	**0.71**	63±16
$\delta^{13}C_{ben}$	**0.74**	36±15	**0.77**	125±14	0.48	−167±30	**0.94**	−121±6	0.63	−44±20	**0.70**	−48±17	0.51	−93±28
Mediterranean														
$\delta^{18}O_{plan}$	**0.89**	−11±8	**0.78**	0±13	**0.84**	27±10	**0.92**	48±7	**0.97**	58±4	**0.98**	60±3	**0.98**	69±3
$\delta^{13}C_{plan}$	**0.91**	5±8	**0.73**	4±15	0.59	−58±22	**0.80**	−59±12	**0.94**	83±6	**0.86**	57±10	**0.91**	77±7
ODP Site 1143														
$\delta^{18}O_{ben}$	0.38	−62±41	0.64	13±19	**0.75**	31±15	**0.94**	39±6	**0.83**	47±11	**0.90**	71±8	**0.90**	78±8
$\delta^{13}C_{ben}$	0.62	47±20	**0.68**	93±18	0.50	173±29	**0.95**	−113±6	0.43	−121±34	**0.78**	−82±13	0.60	−70±22
$\delta^{18}O_{plan}$	0.19	−13±94	0.32	44±50	0.50	92±28	**0.79**	40±12	**0.78**	22±13	0.62	76±21	0.33	22±48
$\delta^{13}C_{plan}$	0.38	−131±40	0.52	88±27	0.50	−171±28	**0.89**	−80±8	0.37	−25±42	0.52	−56±27	0.61	−70±21
Site 659														
$\delta^{18}O_{ben}$	**0.77**	−25±13	0.63	−14±20	**0.77**	11±13	**0.86**	35±10	**0.84**	44±11	0.63	46±20	**0.77**	70±13
$\delta^{13}C_{ben}$	**0.77**	26±14	**0.77**	123±13	0.43	176±35	**0.88**	−132±9	**0.76**	−93±14	0.30	−66±54	**0.75**	−55±14

Coherence indicated in bold means at 99% significance level; phase (pha) in degrees; error bars estimated at 90% confidence limits.

This may also explain the almost in-phase relationship between the 400-kyr components of the isotope records in the Mediterranean planktonic record and long eccentricity cycles (Tables 2 and 3). This interpretation is in agreement with simple energy balance model simulations that show that the largest thermal response to the precession cycles is seen over Africa (Short and Mengel, 1986), and that the interaction between the twice-yearly passage of the sun across the equator and the seasonal timing of perihelion increase the tropical climate response to the eccentricity cycles, implying a strong response of the African monsoon to the 400, 125 and 95-kyr cycles (Short et al., 1991; Crowley et al., 1992).

4.2. Pleistocene obscuring of long eccentricity cyclicity in $\delta^{13}C$ records

The frequency change in the deep marine $\delta^{13}C$ records from regular 400-kyr cyclicity in the Pliocene to an approximately 500-kyr beat during the last million years has previously been notified (Wang et al., 2003, 2004). It appeared that middle and late Pleistocene long-term $\delta^{13}C$max events do not correspond unequivocally to eccentricity minima as for the Pliocene, but occur at high eccentricity values; $\delta^{13}C$max-II at 0.5 Ma and $\delta^{13}C$max-III at 1.0 Ma (Fig. 4B; Wang et al., 2004). It was argued that the obscured 400-kyr $\delta^{13}C$ signal during the Pleistocene is mainly driven by the global climate deterioration and

Table 3
Cross-spectral results between ETP* and stable isotope records (0–1.6 Ma).

	Eccentricity								
	400 kyr			125 kyr			95 kyr		
	coh	pha	Time lag	coh	pha	Time lag	coh	pha	Time lag
Leg 154									
$\delta^{18}O_{ben}$	0.69	−3±21	−3±23	**0.84**	2±13	1±4	0.71	11±19	3±5
$\delta^{13}C_{ben}$	0.49	−166±36	−185±39	**0.79**	159±15	55±5	0.47	165±37	43±10
Leg 138									
$\delta^{18}O_{ben}$	0.23	53±91	59±101	**0.89**	20±10	7±4	0.69	15±20	4±5
$\delta^{13}C_{ben}$	0.32	−77±59	−86±66	**0.81**	157±14	54±5	0.67	160±22	42±6
Mediterranean									
$\delta^{18}O_{plan}$	**0.82**	1±14	1±15	**0.80**	4±15	1±5	0.75	9±17	2±5
$\delta^{13}C_{plan}$	**0.82**	−46±13	−51±15	0.69	−29±20	−10±7	0.76	−118±17	−31±4
ODP Site 1143									
$\delta^{18}O_{ben}$	0.76	36±17	40±18	0.84	19±13	7±4	0.74	15±18	4±5
$\delta^{13}C_{ben}$	0.31	168±62	187±69	0.74	106±18	37±6	0.76	164±17	43±4
$\delta^{18}O_{plan}$	0.56	40±29	44±32	0.60	28±26	10±9	0.45	62±39	16±10
$\delta^{13}C_{plan}$	0.50	−135±34	−150±38	0.60	120±26	42±9	0.87	147±11	39±3
Site 659									
$\delta^{18}O_{ben}$	0.34	49±55	54±61	0.77	8±16	3±6	0.72	−2±19	−1±5
$\delta^{13}C_{ben}$	0.22	−66±97	−74±108	0.64	137±24	48±8	0.65	136±23	36±6

Coherence indicated in bold means at 99% significance level; phase (pha) in degrees; error bars estimated at 90% confidence limits.

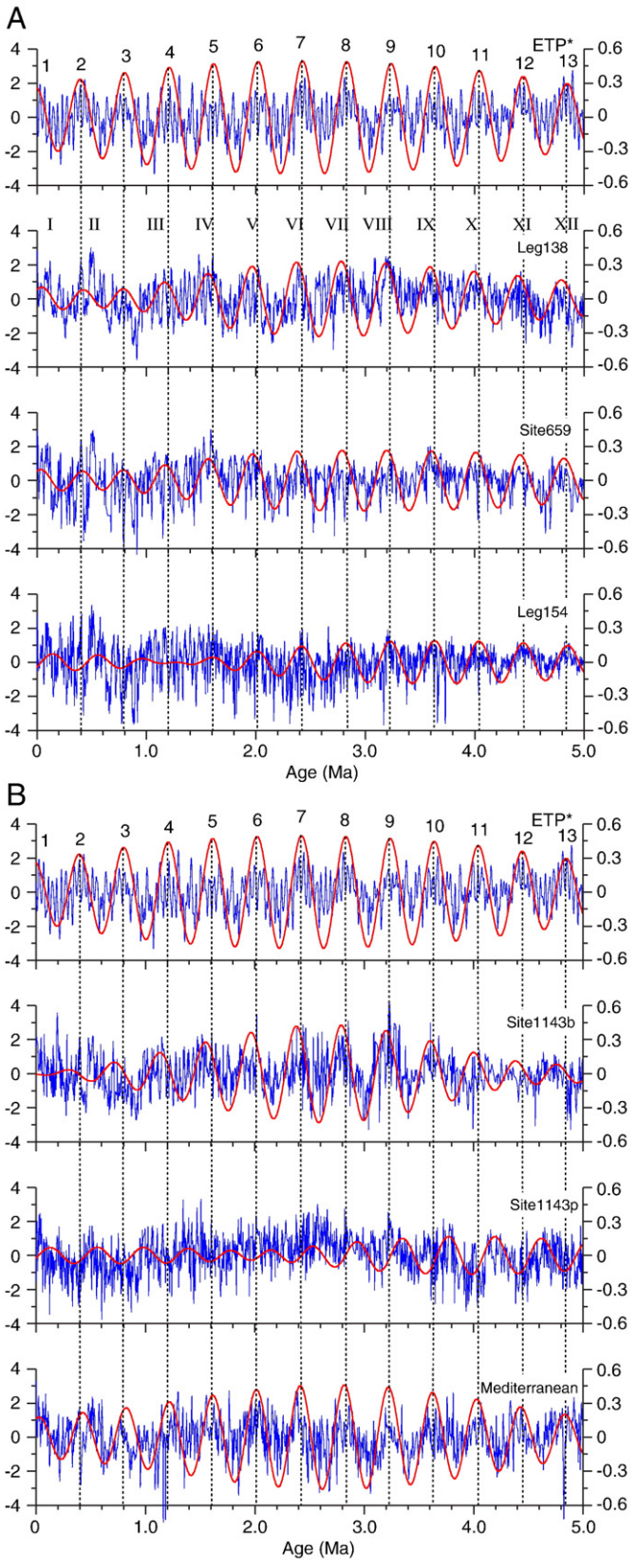

Fig. 3. Comparison between the normalized δ^{13}C time series of the past 5.0 Ma, ETP* and their filtered 400-kyr (long eccentricity) components: (A) data from Leg 138 and 154 and Site 659; (B) data from the Mediterranean and Site 1143. See text for further explanations. Numbers 1–13 denote long eccentricity minima, I–XII mark δ^{13}Cmax.

the overriding influence of the 41-kyr and 100-kyr glacial cycles on the open ocean δ^{13}C records (Wang et al., 2004). There is for instance no astronomical reason for the absence of a δ^{13}C maximum at the long eccentricity minimum at 0.8 Ma. Probably this discrepancy is related to the sharp ~0.3‰ decrease in mean ocean δ^{13}C around 0.9–1.0 Ma (Raymo et al., 1997), which may have led to the Mid-Pleistocene Revolution (MPR) around 0.9 Ma (Wang et al., 2004). Presumably, a drastic change took place in the oceanic carbon reservoir related to the onset of the 100-kyr dominated glacial world that perturbed the δ^{13}C response to the long eccentricity cycle.

Similarly, the failure of isotopic response to the eccentricity minimum at 0.4 Ma originated from the δ^{13}Cmax-II event at ~0.5 Ma. Again, the δ^{13}Cmax-II was followed by a significant negative δ^{13}C shift, preceding a major expansion of ice-sheet size at the beginning of the "Mid-Brunhes Event" (Wang et al., 2003). Both δ^{13}Cmax-II and δ^{13}Cmax-III events were accompanied by extremely enhanced monsoon and humidity conditions in the low latitudes: The δ^{13}Cmax-II event (MIS 13) was accompanied by unusual freshwater discharge to the Indian Ocean (event Y; Bassinot et al., 1994b), extraordinarily high terrigenous flux in the Amazon Basin (Harris et al., 1997), and the strongest chemical weathering of paleosol S5-1 in the Chinese Loess Plateau (Guo et al., 1998) (Fig. 9 in Wang et al., 2004). Similarly, the δ^{13}Cmax-III event (MIS 27–29) coevaled with a sudden decrease of *Spimiferites* in dinoflagellate assemblages off Congo estuary (Dupont et al., 2001), a major change in $CaCO_3$% off the Amazon estuary (Bassinot et al., 1997) and in aragonite % at the Maldivas (Droxler et al., 1990), probably related to enhanced precipitation in the tropics (Fig. 10 in Wang et al., 2004). However, high-latitude processes must have played a crucial role in the carbon shift following these δ^{13}Cmax events. An example is the strong ~1.0‰ negative excursion during MIS 12, which is only observed in benthic (Fig. 1F, H, and J) but not in planktonic δ^{13}C records (Fig. 1B and D). This excursion represents a drastic change in deep-water circulation preceding the ice-sheet expansion (Wang et al., 2003). Obviously, the series of climate events, from carbon reservoir changes to ice-sheet expansion, perturbed normal pace of the eccentricity forcing of climate as recorded before the Pleistocene.

4.3. Instability of long eccentricity imprint on climate changes

Since the "400-kyr problem" was raised more than two decades ago, paleoclimate scientists have adopted various approaches to find out the 400-kyr signal in the isotope records. For example, Rial (2004) showed that the 400-kyr signal is deeply buried in the δ^{18}O time series, but can be concealed by frequency modulation. However, it just reformulated but not answered the question, because it remains mysterious why the long eccentricity signal becomes "deeply buried" in the Pleistocene.

If we look at low-latitude records, the direct 400-kyr imprint on climate changes is maintained in some proxies in the Pleistocene. Heavy peak values are traceable for instance at 1.2 Ma and 0.8 Ma in some of δ^{13}C series, especially in the Mediterranean (Figs. 1B and 3). In addition, the equatorial Atlantic reveals a dust flux minimum value at ~0.4, along with another minimum at 0.5 Ma (Fig. 4I; Tiedemann et al., 1994). In the equatorial Indian Ocean, the 400-kyr cycles are observed in primary productivity (Beaufort et al., 1997) whereas the δ^{13}C and carbonate records from the same site display 500-kyr cycles (Bassinot et al., 1994a). Obviously, the productivity is a local signal, while the carbonate reservoir change is global or regional in nature. In other words, the 400-kyr long eccentricity is still regulating the intensity of low-latitude processes in the climate system such as monsoons or, in this case, the ENSO-related Indian Ocean equatorial westerlies (Beaufort et al., 1997), when the 400-kyr cycles in the oceanic carbon reservoir were already dampened. Therefore, the Pleistocene obscuring of δ^{13}C records at the long eccentricity band resulted from internal feedback mechanisms inside the ocean–

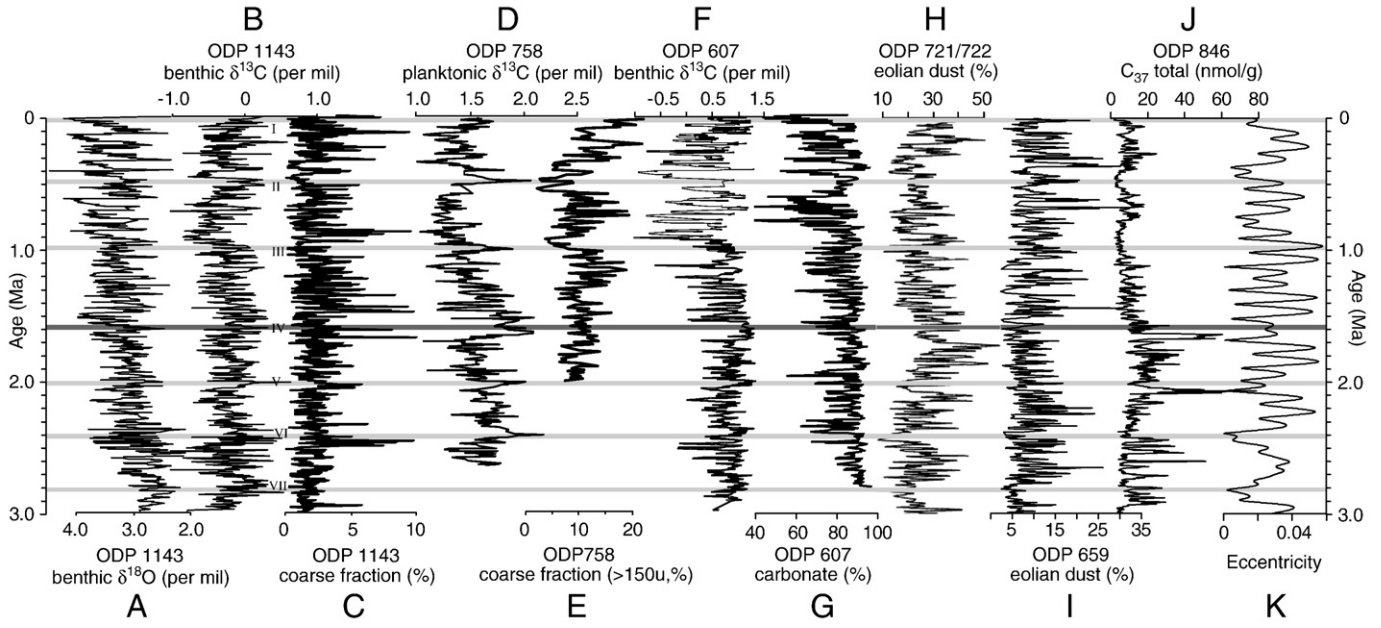

Fig. 4. Long eccentricity cycles in carbon isotope and paleoenvironmental records over the past 3 Ma. (A) benthic $\delta^{18}O$, (B) benthic $\delta^{13}C$ and (C) coarse fraction (%) at ODP 1143, South China Sea (Wang et al., 2003, 2004); (D) planktonic $\delta^{13}C$ and (E) coarse fraction % at ODP 758, Indian Ocean (Schmidt et al., 1993; Bassinot et al., 1994a); (F) benthic $\delta^{13}C$ and (G) carbonate % at ODP 607, North Atlantic (Ruddiman et al., 1989; Raymo et al., 1989); (H) aeolian detritus % at ODP 721/722, Arabian Sea (DeMenocal, 1995); (I) dust flux (g/m^2/yr) at ODP 659, eastern equatorial Atlantic (Tiedemann et al., 1994); (J) concentration of C_{37} alkenones (nmol/g) at ODP 846, equatorial Pacific (Lawrence et al., 2006). Grey bars and Roman numbers indicate $\delta^{13}C$max (I–IIV).

atmosphere–biosphere system, whereas the eccentricity forcing of the tropical processes remains stable.

The 1.6 Ma transition affects not only the long, 400-kyr, but also the short, 100-kyr, eccentricity-related signal. Before the Pleistocene, during the Oligocene–Miocene for example, $\delta^{13}C$ and $\delta^{18}O$ are more or less in phase with eccentricity in both the 400 and 100 kyr bands, with only 18–60 degree lag (Table 1 in Zachos et al., 2001), whereas during the Pleistocene, the phase relations for the benthic isotope records became clearly in anti-phase for the 100 kyr band (Table 3). In other words, the phase relations for the 100-kyr band are starting to show a similar anti-phase behavior as found for the 41-kyr (obliquity) component. The anti-phase relationship for the obliquity cycle is clearly detected in the benthic records of the past 5 Myr (Table 2) and can be explained by the large imprint of glacial cyclicity, as during full glacial conditions benthic $\delta^{18}O$ increases due to temperature and ice volume, while $\delta^{13}C$ decreases due to less continental vegetation, sluggish THC and so on. When the glacials start to follow a 100-kyr rhythm, the benthic isotope records show exactly a similar phase behavior as for the 41-kyr cycle. Thus, when the in-phase 100-kyr relationship between $\delta^{18}O$ and $\delta^{13}C$ shifts to an anti-phase relationship we see a decoupling of the 400-kyr eccentricity component.

4.4. Two response models of oceanic carbon reservoir to eccentricity forcing

Intriguingly, the obscuring of long eccentricity signal in isotopic records is not restricted to the Pleistocene, and the 400-kyr cycles in $\delta^{13}C$ have been interrupted earlier in the Cenozoic. An example is the Middle Miocene cooling event associated with expansion of the Antarctic ice sheet. At the end of Middle Miocene deposition of the Monterey Formation, an abrupt cooling event at 13.9 Ma is accompanied by a sudden disappearance of 400-kyr cycles in $\delta^{13}C$ records (Fig. 4A) (Holbourn et al., 2005, 2007; Tian et al., 2009). This implies that the eccentricity cycle is constantly affecting the oceanic carbon reservoir but not always prominent in deep ocean $\delta^{13}C$ records.

The obscuring of long eccentricity signal in $\delta^{13}C$ records at ~1.6 Ma is not accidental, but resulted from a reorganization of the ocean structure. About 1.6 Ma, glacial $\delta^{13}C$ values in the Southern Ocean became significantly lower than those in the deep Pacific (Venz and Hodell, 2002), and the difference between intermediate and deep-water $\delta^{13}C$ increased between 2.75 and 1.55 Ma, suggesting enhancement of the chemical divide separating the intermediate and deep waters in the southern Ocean (Hodell and Venz-Curtis, 2006). Since the modern Southern Ocean is the most important region in controlling atmospheric CO_2 and serves as "a lid to a larger volume of the deep ocean" (Marinov et al., 2006), the final formation of the chemical divide 1.6 Myr ago has greatly enhanced the role of the Southern Ocean in global carbon cycling. Indeed, the occurrences of $\delta^{13}C$max after 1.6 Ma are tightly related to significant changes in the Southern Ocean. For example, the $\delta^{13}C$max-II about 0.5 Ma was preceded by deposition of thick monospecific diatom layers 0.544–0.534 Ma (Gingele and Schmieder, 2001) suggesting seepage of the Si-rich water from the Southern Ocean. Similarly, the occurrence of $\delta^{13}C$max-III at about 1.0 Ma followed the Super-Interglacial MIS 31 at1.06 Ma when the Western Antarctic ice sheet collapsed (Pollard and DeConto, 2009).

The restructure of ocean water in the high-latitude ocean has also led to a new pattern of upper structure in the equatorial ocean (Fedorov et al., 2006). Recent studies found that east–west asymmetry of the modern tropical Pacific Ocean SST and thermocline depth was established about 1.6 Ma, finally terminating the permanent El Niño-like conditions of the Pliocene (Wara et al., 2005; Lawrence et al., 2006; Ravelo et al., 2006). Moreover, the ocean water restructure at 1.6 Ma also exerted an impact on the climate response to orbital forcing (Lisiecki and Raymo, 2005).

Although the mechanism behind all the above described chain of changes at 1.6 Ma remains elusive and much more work is needed for its exploration, it is clear that the Southern Ocean played a critical role, and the oceanic carbon reservoir responds to eccentricity forcing differently with or without large polar ice sheets. Hypothetically, we can distinguish two models of response: In an ice-free or one-pole ice-caped Earth, both the oceanic benthic $\delta^{18}O$ and $\delta^{13}C$ are responding to eccentricity cycles through modulation of the precession-driven low-latitude processes (Wang et al., 2004; Wang, 2009). With the

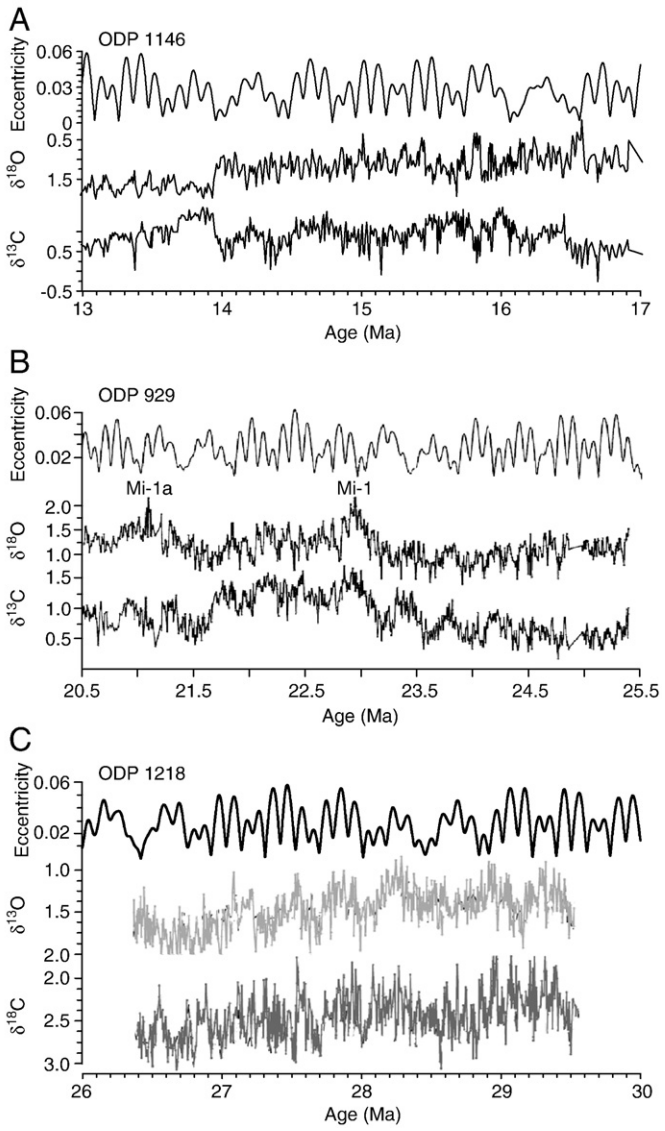

Fig. 5. Examples of 400-kyr cycles of long eccentricity in benthic foraminifer $\delta^{18}O$ and $\delta^{13}C$ records. (A) Middle Miocene, 13–17 Ma, ODP 1146, South China Sea (Holbourn et al., 2004). (B) Oligocene–Miocene boundary, 20–23.4 Ma, ODP 929, Ceara Rise (Paul et al., 2000). (C) Oligocene, 26–30 Ma, ODP 1218, equatorial Pacific (Wade and Pälike, 2004).

development of large bi-polar ice sheets, the $\delta^{13}C$ response to eccentricity is obscured by the major reorganizations of the ocean circulation, whereas the eccentricity modulation of the precession-driven low-latitude processes maintains as seen in $\delta^{13}C_{plan}$ record of the Mediterranean basin because of its isolation from the deep-water circulation of the global ocean.

The key to the long eccentricity question lies in the δ^{13}Cmax events. We have to find out what happened in the Earth system at δ^{13}Cmax, and by what mechanism the long eccentricity minimum leads to δ^{13}Cmax in the oceanic carbon reservoir. Of particular importance is to understand the δ^{13}Cmax in the Pleistocene. Unlike the δ^{13}Cmax before 1.6 Ma directly driven by astronomical forcing, the late Quaternary δ^{13}Cmax events were obviously related to internal feedback of the ocean and climate system. This is revealed by the fact that the Atlantic (Fig. 4G) and Indo-Pacific Oceans (Fig. 4C, E) displayed opposite trends in carbonate preservation between the δ^{13}Cmax events. Nonetheless, the δ^{13}Cmax of different origin share similar features in the long-term cycles of the oceanic carbon reservoir. If the past two Pleistocene δ^{13}Cmax at 0.5 and 1.0 Ma were out of phase with long eccentricity minimum, but followed by rigorous ice-sheet expansion, what does the current δ^{13}Cmax mean for the Earth system? This new δ^{13}Cmax corresponds to eccentricity minimum, our scientific concern should be not limited to the reduced amplitude of climate precession, an urgent task is to decipher the long eccentricity cycle in oceanic carbon reservoir.

Table 4
Comparison between carbon isotope maximum events in the open ocean and eccentricity minima over the last 5 Myr.

Eccentricity minimum No.	Age (Ma)	δ^{13}Cmax No.	Age (Ma)	δ^{18}O MIS	Reference
1	Present	I	0–0.05	1–3	Wang et al. (2004)
2	0.395	II	0.47–0.53	13	
3	0.802	III	0.95–1.00	25–27	
4	1.209				
5	1.615	IV	1.55–1.65	53–57	
6	2.021	V	2.00–2.06	75–77	Wang et al. (2003)
7	2.427	VI	2.38–2.44	93–95	
8	2.832	VII	2.73–2.80	G7–G9	
9	3.237	VIII	3.20–3.29	KM5–M1	
10	3.640	IX	3.56–3.61	Gi1	
11	4.042	X	3.97–4.01	Gi20	This paper
12	4.444	XI	4.39–4.42	CN6	
13	4.846	XII	4.75–4.82	NS6–Si2	

5. Conclusions

1. The 400-kyr cycles of long eccentricity are observed in Pliocene $\delta^{13}C$ records from open and marginal settings, with δ^{13}Cmax occurring at eccentricity minimum.
2. Since ~1.6 Ma the long eccentricity is obscured in the deep ocean $\delta^{13}C$ records, suggesting a major change in the oceanic carbon reservoir probably associated with a glacial-induced restructure of the Southern Ocean.
3. As the Earth is now passing through another δ^{13}Cmax and eccentricity minimum stage, it is crucial to reveal the nature of δ^{13}Cmax events and its impact on ice-sheet changes. It is impossible to scientifically predict the future long-term trend of the climate without understanding the impact of long eccentricity cycle on the Earth system.

Acknowledgement

The authors express their gratitude to anonymous reviewers for their critical comments and constructive advices which helped to improve the manuscript. Dr. Qianyu Li is acknowledged for discussions and comments on an early version of the manuscript. This research used samples and data provided by the Ocean Drilling Program [ODP]. ODP is sponsored by the U.S. National Science Foundation [NSF] and participating countries under management of Joint Oceanographic Institutions [JOI], Inc. This work was supported by the National Basic Research Program of China (Grant No. 2007CB815902).

Appendix A. Supplementary data

Supplementary data associated with this article can be found, in the online version, at doi:10.1016/j.epsl.2009.12.028.

References

Bassinot, F.C., Beaufort, L., Vincent, E., Labeyrie, L., F., Rostek, Muller, P.J., Quidelleur, X., Lancelot, Y., 1994a. Coarse fraction fluctuations in pelagic carbonate sediments from the tropical Indian Ocean: a 1500-kyr record of carbonate dissolution. Paleoceanography 9, 579–600.

Bassinot, F.C., Labeyrie, L.D., Vincent, E., Quidelleur, X., Shackleton, N.J., Lancelot, Y., 1994b. The astronomical theory of climate and the age of the Brunhes–Matuyama magnetic reversal. Earth Planet. Sci. Lett. 126, 91–108.

Bassinot, F.C., Beaufort, L., Vincent, E., Labeyrie, L., 1997. Changes in the dynamics of Western equatorial Atlantic surface currents and biogenic productivity at the "Mid-Pleistocene Revolution" (930 ka). Proc. Ocean Drilling Program Sci. Results 154, 269–284.
Beaufort, L., Lancelot, Y., Camberlin, P., Cayre, O., Vincent, E., Bassinot, F., Labeyrie, L., 1997. Insolation cycles as a major control of equatorial Indian Ocean primary production. Science 278, 1451–1454.
Berger, A., Loutre, M.F., 1991. Insolation values for the climate of the last 10 million years. Quat. Sci. Rev. 10, 297–317.
Bickert, T., Curry, W.B., Wefer, G., 1997. Late Pliocene to Holocene (2.6–0 Ma) western equatorial Atlantic deep-water circulation: inferences from benthic stable isotopes. In: Shackleton, N.J., Curry, W.B., Richter, C., Bralower, T.J. (Eds.), Proc. ODP, Sci. Results, vol. 154, pp. 239–253.
Billups, K., Ravelo, A.C., Zachos, J.C., 1997. Early Pliocene deep-water circulation: stable isotope evidence for enhanced northern component deep water. In: Shackleton, N.J., Curry, W.B., Richter, C., Bralower, T.J. (Eds.), Proc. ODP, Sci. Results, vol. 154, pp. 319–330.
Billups, K., Pälike, H., Channell, J.E.T., Zachos, J.C., Shackleton, N.J., 2004. Astronomic calibration of the late Oligocene through early Miocene geomagnetic polarity time scale. Earth Planet. Sci. Lett. 224, 33–44.
Briskin, M., Berggren, W.A., 1975. Pleistocene stratigraphy and quantitative paleoceanography of tropical North Atlantic core V16-205. In: Saito, T., Burckle, L. (Eds.), Late Neogene Epoch Boundaries. Micropaleontol. Press, New York, pp. 167–198.
Chen, J., Farrell, J.W., Murray, D.W., Prell, W.L., 1995. Timescale and paleoceanographic implications of a 3.6 m.y. oxygen isotope record from the northeast Indian Ocean (Ocean Drilling Program Site 758). Paleoceanography 10, 21–47.
Clemens, S.C., Tiedemann, R., 1997. Eccentricity forcing of Pliocene–Early Pleistocene climate reveled in a marine oxygen-isotope record. Nature 385, 801–804.
Cramer, B.S., Wright, J.D., Kent, D.V., Aubry, M.-P., 2003. Orbital climate forcing of $\delta^{13}C$ excursions in the late Paleocene–early Eocene (chrons C24n–C25n). Paleoceanography 18. doi:10.1029/2003PA000909.
Crowley, T.J., Kim, K.-Y., Mengel, J.G., Short, D.A., 1992. Modeling 100,000-year climate fluctuations in Pre-Pleistocene time series. Science 255, 705–707.
DeMenocal, P.B., 1995. Plio-Pleistocene African climate. Science 270, 53–59.
DeMenocal, P., Archer, D., Leth, P., 1997. Pleistocene variations in deep Atlantic circulation and calcite burial between 1.2 and 0.6 Ma: a combined data-model approach. In: Shackleton, N.J., Curry, W.B., Richter, C., Bralower, T.J. (Eds.), Proc. ODP, Sci. Results, vol. 154, pp. 285–298.
Droxler, A.W., Haddad, G.A., Mucciarone, D.A., Cullen, J.L., 1990. Pliocene–Pleistocene aragonite cyclic variations in Holes 714A and 716B (the Maldives) compared with Hole 633A (the Bahamas): records of climate-induced $CaCO_3$ preservation at intermediate water depths. Proc. Ocean Drilling Program Sci. Results 115, 539–577.
Dupont, L.M., Donner, B., Schneider, R., Wefer, G., 2001. Mid-Pleistocene environmental change in tropical Africa began as early as 1.05 Ma. Geology 29, 195–198.
Farrell, J.W., Janecek, T.R., 1991. Late Neogene paleoceanography and paleoclimatology of the northeast Indian Ocean (Site 758). Proc. Ocean Drilling Program Sci. Results 121, 297–355.
Fedorov, A.V., Dekens, P.S., McCarthy, M., Ravelo, A.C., deMonical, P.B., Barreiro, M., Pacanowski, R.C., Philander, S.G., 2006. The Pliocene paradox (mechanisms for a permanent El Nino). Science 312, 1485–1489.
Fontugne, M.R., Calvert, S.E., 1992. Late Pleistocene variability of the carbon isotopic composition of organic matter in the eastern Mediterranean: monitor of changes in carbon sources and atmospheric CO_2 concentrations. Paleoceanography 7 (1), 1–20.
Franz, S.O., Tiedemann, R., 1997. Physical and chemical changes of deep-water masses between 3000–4400 m water depth in the equatorial W-Atlantic during the Pliocene (ODP Leg 154, Ceara Rise). Development of Paleoceanography as a New Field of Science, 50th Anniversary of the Albatross Expedition 1947 – 1948, vol. 50. Royal Swedish Academy of Science, Stockholm, Schweden. Abstract.
Gingele, F.X., Schmieder, F., 2001. Anomalous South Atlantic lithologies confirm global scale of unusual mid-Pleistocene climate excursion. Earth Planet. Sci. Lett. 186, 93–101.
Gudjonsson, L., van der Zwaan, G.J., 1985. Anoxic events in the Pliocene Mediterranean: stable isotope evidence of run-off. Proc. K. Ned. Akad. Wet., Ser. B 88 (1), 69–82.
Guo, Z., Liu, T., Fedoroff, N., Wei, L., Ding, Z., Wu, N., Lu, H., Jiang, W., An, Z., 1998. Climate extremes in Loess of China coupled with the strength of deep-water formation in the North Atlantic. Global Planet. Change 18, 113–1228.
Harris, S.E., Mix, A.C., King, T., 1997. Bogenic and terrigenous sedimentation at Ceara Rise, western tropical Atlantic, supports Pliocene–Pleistocene deep-water linkage between hemisphere. Proc. Ocean Drilling Program Sci. Results 154, 331–345.
Hilgen, F.J., 1991. Astronomical forcing and geochronological application of sedimentary cycles in the Mediterranean Pliocene–Pleistocene. Ph.D thesis. Geologica Ultraiectina. Mededelingen van de Faculteit Aardwetenschappen der Universiteit Utrecht. No.93, 1-139.
Hodell, D.A., Venz-Curtis, K.A., 2006. Late Neogene history of deepwater ventilation in the Southern Ocean. Geochem. Geophys. Geosyst. 7, Q09001. doi:10.1029/2005GC001211.
Holbourn, A., Kuhnt, W., Schulz, M., 2004. Orbitally paced climate variability during the Middle Miocene: high resolution benthic foraminiferal stable-isotope records from the tropical Western Pacific. In: Clift, P., et al. (Ed.), Continent–Ocean Interactions within East Asian Marginal Seas. Geophys. Monogr. Ser., vol. 149. AGU, pp. 321–337.
Holbourn, A., Kuhnt, W., Schulz, M., Erlenkeuser, H., 2005. Impacts of orbital forcing and atmospheric carbon dioxide on Miocene ice-sheet expansion. Nature 438, 483–487.
Holbourn, A., Kuhnt, W., Schulz, M., Flores, J.-A., Andersen, N., 2007. Orbitally-paced climate evolution during the middle Miocene "Monterey" carbon-isotope excursion. Earth Planet. Sci. Lett. 261, 534–550.
Hoogakker, B.A.A., Rohling, E.J., Palmer, M.R., Tyrrell, T., Rothwell, R.G., 2006. Underlying causes for long-term global ocean $\delta^{13}C$ fluctuations over the last 1.20 Myr. Earth Planet. Sci. Lett. 248, 15–29.
Imbrie, J., Imbrie, J.Z., 1980. Modeling the climatic response to orbital variations. Science 207, 943–953.
Imbrie, J., Boyle, E., Clemens, S., et al., 1992. On the structure and origin of major glaciation cycles, 1, Linear responses to Milankovitch forcing. Paleoceanography 7, 701–738.
Katz, M.E., Wright, J.D., Miller, K.G., Cramer, B.S., Fennel, K., Falkowski, P.G., 2005. Biological overprint of the geological carbon cycle. Mar. Geol. 217, 323–338.
Kent, D.V., Olsen, P.E., 1999. Astronomically tuned geomagnetic polarity timescale for the Late Triassic. J. Geophys. Res. 104, 12831–12841.
Kroon, D., Alexander, I., Little, M., Lourens, L.J., Matthewson, A., Robertson, A.H.F., Sakamoto, T., 1998. Oxygen isotope and sapropel stratigraphy in the eastern Mediterranean during the last 3.2 million years. In: Robertson, A.H.F., Emeis, K.-C., Richter, C., Camerlenghi, A. (Eds.), Proc. ODP Sci. Results, vol. 160, pp. 181–189.
Laskar, J., 1988. Secular evolution of the Solar System over 10 million years. Astron. Astrophys. 198, 341–362.
Laskar, J., 1990. The chaotic motion of the solar system: a numerical estimate of the size of the chaotic zones. Icarus 88, 266–291.
Laskar, J., Robutel, P., Joutel, F., et al., 2004. A long term numerical solution for the insolation quantities of the Earth. Astron. Astrophys. 428, 261–285.
Lawrence, K.T., Liu, Z., Herbert, T.D., 2006. Evolution of the Eastern Tropical Pacific through Plio-Pleistocene glaciation. Science 312, 79–83.
Lisiecki, L.E., Raymo, M.E., 2005. A Pliocene–Pleistocene stack of 57 globally distributed benthic $\delta^{18}O$ records. Paleoceanography 20. doi:10.1029/2004PA001071.
Lourens, L.J., 2004. Revised tuning of Ocean Drilling Program Site 964 and KC01B (Mediterranean) and implications for the delta O-18, tephra, calcareous nannofossil, and geomagnetic reversal chronologies of the past 1.1 Myr. Paleoceanography 19 (3), PA3010. doi:10.1029/2003PA000997.
Lourens, L.J., Antonarakou, A., Hilgen, F.J., Van Hoof, A.A.M., Vergnaud-Grazzini, C., Zachariasse, W.J., 1996a. Evaluation of the Plio-Pleistocene astronomical timescale. Paleoceanography 11, 391–413.
Lourens, L.J., Hilgen, F.J., Raffi, I., Vergnaud-Grazzini, C., 1996b. Early Pleistocene chronology of the Vrica section (Calabria, Italia). Paleoceanography 11, 797–812.
Lourens, L.J., Hilgen, F.J., Shackleton, N.J., Laskar, J., Wilson, D., 2004. The Neogene period. In: Gradstein, et al. (Ed.), A Geologic Time Scale 2004. Cambridge University Press, pp. 409–440.
Lourens, L.J., Sluijs, A., Kroon, D., Zachos, J.C., Thomas, E., Röhl, U., Bowles, J., Raffi, I., 2005. Astronomical pacing of late Palaeocene to early Eocene global warming events. Nature 435, 1083–1087.
Marinov, I., Gnanadesikan, A., Toggweiler, J.R., Sarmiento, J.L., 2006. The Southern Ocean biogeochemical divide. Nature 441, 964–967.
Matthews, R.K., Froelich, C., 2002. Maximum flooding surfaces and sequence boundaries: comparisons between observations and orbital forcing in the Cretaceous and Jurassic (65–190 Ma). GeoArabia, Middle East Petrol. Geosci. 7, 503–538.
Mix, A.C., Le, J., Shackleton, N.J., 1995a. Benthic foraminifer stable isotope stratigraphy of Site 846: 0–1.8 Ma. In: Palmer-Julson, A., van Andel, T.H. (Eds.), Proc. ODP, Sci. Res., vol. 138, pp. 839–856.
Mix, A.C., Pisias, N.G., Rugh, W., Wilson, J., Morey, A., Hagelberg, T.K., 371–412, 1995b. Benthic foraminifer stable isotope record from Site 849 (0–5 Ma): local and global climate changes. In: Pisias, N.G., Mayer, L., Janecek, T., Palmer-Julson, A., van Andel, T.H. (Eds.), Proc. Ocean Drilling Program Sci. Results, vol. 138, pp. 371–412.
Mohtadi, M., Hebbeln, D., Ricardo, S.N., Lange, C.B., 2006. El Niño-like pattern in the Pacific during marine isotope stages (MIS) 13 and 11? Paleoceanography 21, PA1015. doi:10.1029/2005PA001190.
Olsen, P.E., 1986. A 40 million-year lake record of early Mesozoic climatic forcing. Science 234, 842–848.
Paillard, D., Labeyrie, L., Yiou, P., 1996. Macintosh program performs time-series analysis. Eos Trans. AGU 77, 379.
Pälike, H., Norris, R.D., Herrle, J.O., Wilson, P.A., Coxall, H.K., Lear, C.H., Shackleton, N.J., Tripati, A.K., Wade, B.S., 2006. The heartbeat of the Oligocene climate system. Science 314, 1894–1898.
Paul, H.A., Zachos, J.C., Flower, B.P., Tripati, A., 2000. Orbitally induced climate and geochemical variability across the Oligocene/Miocene boundary. Paleoceanography 15 (71), 485.
Pollard, D., DeConto, R.M., 2009. Modelling West Antarctic ice sheet growth and collapse through the past five million years. Nature 458, 329–333.
Ravelo, A.C., Dekens, P.S., McCarthy, M., 2006. Evidence for El Nino-like conditions during the Pliocene. GSA Today 16 (3). doi:10.1130/1052-5173(2006) 016.
Raymo, M.E., Ruddiman, W.F., Backman, J., Clement, B.M., Martinson, D.G., 1989. Late Pliocene variation in Northern Hemisphere ice sheets and North Atlantic deep water circulation. Paleoceanography 4, 413–446.
Raymo, M.E., Oppo, D.W., Curry, W., 1997. The mid-Pleistocene climate transition: a deep sea carbon isotopic perspective. Paleoceanography 12, 546–559.
Rial, J.A., 2004. Earth's orbital eccentricity and the rhythm of the Pleistocene ice ages: the concealed pacemaker. Global Planet. Change 41, 81–93.
Rohling, E.J., Hilgen, F.J., 1991. The eastern Mediterranean climate at times of sapropel formation: a review. Geol. Mijnbouw 70, 253–264.
Rossignol-Strick, M., 1983. African monsoon, an immediate climate response to orbital insolation. Nature 304, 46–49.
Rossignol-Strick, M., Paterne, M., 1999. A synthetic pollen record of the eastern Mediterranean sapropels of the last 1 Ma: implications for the time-scale and formation of sapropels. Mar. Geol. 153, 221–237.
Ruddiman, W.F., Raymo, M.E., Martinson, D.G., Clement, B.M., Backman, J., 1989. Pleistocene evolution: Northern Hemisphere ice sheets and North Atlantic Ocean. Paleoceanography 4, 353–412.

Schmidt, H., Berger, W.H., Bickert, T., Wefer, G., 1993. Quaternary carbon isotope record of pelagic foraminifers: Site 806, Ontong Java Plateau. Proc. Ocean Drilling Program Sci. Results 130, 397–409.
Shackleton, N.J., Hall, M.A., 1997. The late Miocene stable isotope record, Site 926. In: Shackleton, N.J., Curry, W.B., Richter, C., Bralower, T.J. (Eds.), Proc. ODP, Sci. Results, vol. 154, pp. 367–374.
Shackleton, N.J., Berger, A., Peltier, W.R., 1990. An alternative astronomical calibration of the lower Pleistocene timescale based on ODP Site 677.Trans. R. Soc. Edinburgh Earth Sci 81, 251–261.
Shackleton, N.J., Hall, M.A., Pate, D., 1995. Pliocene stable isotope stratigraphy of Site 846. In: Pisias, N.G., Mayer, L., Janecek, T., Palmer-Julson, A., van Andel, T.H. (Eds.), Proc. Ocean Drilling Program Sci. Results, vol. 138, pp. 337–355.
Short, D.A., Mengel, J.G., 1986. Tropical climatic phase lags and Earth's precession cycle. Nature 323, 48–50.
Short, D.A., Mengel, J.G., Crowley, T.J., Hyde, W.T., North, G.R., 1991. Filtering of Milankovitch cycles by Earth geography. Quatern. Res. 35, 157–173.
Tian, J., Wang, P., Cheng, X., Li, Q., 2002. Astronomically tuned Plio-Pleistocene benthic δ^{18}O record from South China Sea and Atlantic–Pacific comparison. Earth Planet. Sci. Lett. 203 (1015), 1029.
Tian, J., Shevenell, A., Wang, A., Zhao, Q., Li, Q., Cheng, X., 2009. Reorganization of Pacific Deep Waters linked to middle Miocene Antarctic cryosphere expansion: a perspective from the South China. Palaeogeogr. Palaeoclimatol. Palaeoecol.. doi:10.1016/j.palaeo.2009.10.019.
Tiedemann, R., Franz, S.O., 1997. Deep-water circulation, chemistry, and terrigenous sediment supply in the equatorial Atlantic during the Pliocene, 3.3–2.6 Ma and 5–4.5 Ma. In: Shackleton, N.J., Curry, W.B., Richter, C., Bralower, T.J. (Eds.), Proc. ODP, Sci. Results, vol. 154, pp. 299–318.
Tiedemann, R., Sarnthein, M., Shackleton, N.J., 1994. Astronomic timescale for the Pliocene Atlantic δ^{18}O and dust flux records from Ocean Drilling Program Site 659. Paleoceanography 9, 619–638.
Venz, K.A., Hodell, D.A., 2002. New evidence for changes in Plio-Pleistocene deep-water circulation from Southern Ocean ODP Leg 177 site 1090. Palaeogeogr. Palaeoclimatol. Palaeoecol. 182, 197–220.
Wade, B.S., Pälike, H., 2004. Oligocene climate dynamics. Paleoceanography 19, PA4019. doi:10.1029/2004PA001042.
Wang, P., 2009. Global monsoon in a geological perspective. Chin. Sci. Bull. 54, 1–24.
Wang, P., Tian, J., Cheng, X., Liu, C., Xu, J., 2003. Carbon reservoir change preceded major ice-sheet expansion at the Mid-Brunhes event. Geology 31, 239–242.
Wang, P., Tian, J., Cheng, X., Liu, C., Xu, J., 2004. Major Pleistocene stages in a carbon perspective: the South China Sea record and its global comparison. Paleoceanography 19. doi:10.1029/2003PA000991.
Wara, M.W., Ravelo, A.C., Delaney, M.L., 2005. Permanent El Nino-like conditions during the Pliocene warm period. Science 309, 758–761.
Zachos, J.C., Shackleton, N.J., Revenaugh, J.S., Pälike, H., Flower, B.P., 2001. Climate response to orbital forcing across the Oligocene–Miocene boundary. Science 292, 274–278.